COMPUTER PROGRAM FOR SIMULATING THE SIX-DEGREE-OF-FREEDOM MOTION OF MISSILE DEBRIS FRAGMENTS

Michael J. Hemsch
Nielsen Engineering & Research, Inc., Mountain View, California

ABSTRACT

The rational modeling and empirical correlations used to build a comprehensive computer code for simulating general six-degree-of-freedom motions of missile debris fragments are described. The approach is deterministic in that a number of possible generic fragment shapes were defined, methods were selected to describe the aerodynamic loads on these shapes, and the results were incorporated in a six-degree-of-freedom trajectory program. The method chosen is simple enough to avoid large computation times and yet represents coning and tumbling conditions as well as trimmed flight.

INTRODUCTION

NAVSEA has an extensive program concerned with point defense of targets against incoming missiles. When a defensive weapon system damages an attacking missile, the trajectories of the debris fragments remain of interest, since they may hit the target or nearby areas and cause significant damage. Clearly, the possibility of such an occurrence increases with decreasing intercept distance and with increasing attacker velocity. To determine minimum intercept distances for a given level of probable damage, it is necessary to estimate the trajectories of the various portions of debris following a missile breakup. This requires calculation of the aerodynamic forces and moments over 0-180° angle of attack range and a wide range of flight speeds, angular rates and acceleration conditions. The methods, of course, are also applicable to range safety calculations.

Under contract with NAVSEA, Nielsen Engineering & Research, Inc. (NEAR) has developed engineering methods for prediction of the aerodynamic characteristics of missile debris fragments in six-degree-of-freedom motion. The purpose of this paper is to outline those methods, to describe the resulting computer program, DEBRIS, and to give representative sample calculations.

OVERALL APPROACH

To be useful, the methodology adopted for the simulation of six-degree-of-freedom trajectories of missile fragments must encompass realistic ranges of fragment shapes, attitudes and velocities. Although a very wide range of fragment shapes is possible, this work is concerned with a set of generic shapes which, depending on conditions, could be stable, tumble or trim to a

nonzero angle of attack. Since the various shapes can tumble or trim depending on the relative locations of the fragment center of gravity and aerodynamic center of pressure, the methodology has been designed to compute the fragment aerodynamic characteristics for pitch and yaw angles up to 180° and roll angles up to 360°. Any speed is allowed except that the empirical input for the methods described was developed for the Mach range 0.8 to 3.0.

The fragment shapes for which the methods may be used are shown in Figure 1. Note that there are three basic shapes: (1) a cylindrical body alone with circular cross section and with or without pointed nose; (2) body with one set of identical fins; (3) body with two sets of fins, each set having identical fins. Each finned section may have up to four fins set at arbitrary circumferential positions on the body.

Except for aerodynamics methodology, the basic framework for the computer program was provided by the Science Applications, Inc. (SAI) code known as MAT6. The SAI program consists of a main program, a Runge-Kutta integration subroutine, a routine to perform coordinate transformations and calculate the derivatives of the equations of motion, a table look-up subroutine for computing aerodynamic forces and moments and an autopilot algorithm. A description of the methodology and a list of the program is given in Reference 1. For the purposes of this work the subroutine supplied by SAI for the computation of aerodynamic forces and moments has been replaced by a new routine, GENERIC, and its satellite routines. The new program has been named DEBRIS.

Subroutine GENERIC and its satellite routines represent the methodology derived during the present work. They compute the aerodynamic forces and moments acting on a debris fragment given the kinematic state of the fragment and the local properties of the atmosphere. Most of the computations are done by satellite routines with GENERIC acting, in effect, as a driver program for the force and moment calculations. For a typical case, GENERIC performs the following steps as it builds up the loads for a complete fragment:

(a) Compute forces and moments acting on the fuselage or body of the debris fragment as if no fins were present.

(b) Compute two velocity components at the area centroid of each fin in the wing section. The first component is parallel to the body axis. The second is perpendicular to the plane the fin would occupy if it were not deflected. These velocity components include the increments due to rigid body rotation about the fragment center of gravity.

(c) Compute the "equivalent" angle of attack for each fin in the wing section.

(d) Compute normal force and center of pressure for each wing fin. The equivalent angles of attack computed above are used to determine the fin normal forces based on a wing-alone correlation. A similar approach is used to obtain the fin centers of pressure.

(e) Compute overall forces and moments due to wing section. The methods of Pitts, Nielsen, and Kaattari[2] are used to determine body carryover loads due to the presence of the wing section.

(f) Compute wing-tail interference. At this point, an estimate is made of the interference effects of the wing section on the tail section. This is done by estimating an equivalent angle of attack for each tail fin due to the trailing vortices shed by the wing section. First, an estimate of the strength and location of those vortices over the tail section is made. Then the methods of Reference 2 are used to get the overall downwash. Finally, the appropriate components of that downwash for each fin are computed.

(g) Steps (b) through (e) are repeated for the tail section.

The program is also capable of estimating thrust effects, side forces and moments due to a transverse jet, and out-of-plane side forces and moments due to asymmetric vortex shedding. To gain confidence in the computations for debris fragments, the user can compute the static forces and moments for the complete vehicle configuration (before break-up) and compare those results with available data. Complete details of the methodology are available in Reference 3.

In the rest of the paper, the procedures used for computing body-alone forces and moments, fin equivalent angle of attack, fin forces and wing-tail interference are given. The paper is concluded with example calculations and a summary.

PROCEDURES FOR BODY-ALONE METHOD

The forces and moments acting on a slender body without fins are obtained from slender body theory augmented by the crossflow theory of Allen (Reference 4, Ch. 4). The effects of rigid body rotation about the body center of gravity have been included. However, acceleration terms (i.e. terms dependent on $\dot{u}$, $\dot{v}$, $\dot{w}$, $\dot{p}$, $\dot{q}$, $\dot{r}$) have been neglected. Two physical effects are modeled:

(1) loading due to instantaneous values of the crossflow velocities;

(2) loading due to apparent mass effects which arise when there is a variation of crossflow velocity with axial position on the body axis (Reference 4, Ch. 10).

When crossflow velocities are high enough compared to the axial velocity, flow separation on the leeward side of the body will occur. The effects of separation on the loading of type (1) above are accounted for by including crossflow drag. It is assumed that the type (2) loading above is unaffected by separation. This is equivalent to assuming that the apparent mass for viscous flow over a cross section of the body is the same as for inviscid flow. Since the apparent mass is primarily dependent on the body cross sectional dimension normal to the crossflow and since the separated flow affects this dimension only slightly, the assumption appears to be reasonable.

The appropriate expressions for the forces and moments have been developed previously by Goodwin et al. (Reference 5, eqs. (46)-(49) and (51)-(54)) and are presented below.

$$F_z = -\pi\rho_\infty u \int_0^\ell \frac{d}{dx_s} a^2\left[w - q(x_{s,m} - x_s)\right]dx_s$$
$$-\rho_\infty n c_{d_c} \int_0^\ell a V_{CF}\left[w - q(x_{s,m} - x_s)\right]dx_s \tag{1}$$

$$F_y = -\pi\rho_\infty u \int_0^\ell \frac{d}{dx_s} a^2\left[v + r(x_{s,m} - x_s)\right]dx_s$$
$$-\rho_\infty n c_{d_c} \int_0^\ell a V_{CF}\left[v + r(x_{s,m} - x_s)\right]dx_s \tag{2}$$

$$M = \pi\rho_\infty u \int_0^\ell (x_{s,m} - x_s) \frac{d}{dx_s} a^2\left[w - q(x_{s,m} - x_s)\right]dx_s$$
$$+ \rho_\infty n c_{d_c} \int_0^\ell (x_{s,m} - x_s)\, a V_{CF}\left[w - q(x_{s,m} - x_s)\right]dx_s \tag{3}$$

$$N = -\pi\rho_\infty u \int_0^\ell (x_{s,m} - x_s) \frac{d}{dx_s} a^2\left[v + r(x_{s,m} - x_s)\right]dx_s$$
$$- \rho_\infty n c_{d_c} \int_0^\ell (x_{s,m} - x_s)\, a V_{CF}\left[v + r(x_{s,m} - x_s)\right]dx_s \tag{4}$$

where

$$V_{CF} = \sqrt{[v + r(x_{s,m} - x_s)]^2 + [w - q(x_{s,m} - x_s)]^2}$$

The coordinate system used is shown in Figure 2. It has been assumed that c_{d_c} is independent of position along the body axis. This assumption requires that the variations along the body of crossflow Mach number and Reynolds number not be significant or

$$r(x_{s,m} - x_s) \ll v$$
$$q(x_{s,m} - x_s) \ll w \tag{5}$$

These two assumptions essentially say that the increment in velocity at any point on the body due to body rotation is small compared to the translational velocity of the body. A quick check on this can be made by considering a five foot long body traveling at sonic speed, say 1,000 feet per second. If

the center of rotation is midway along the body, the rotational speed necessary for the maximum rotational velocity increment to reach ±10% of the flight speed is given by

$$q = 0.1 \frac{w}{(x_{s,m} - x_s)}$$

$$= \frac{(0.1)(1000 \text{ ft/sec})}{2.5 \text{ ft}}$$

$$= 40 \text{ radians per second}$$

$$= 382 \text{ RPM}$$

Clearly, it is reasonable to assume that actual rotational speeds will not exceed this value. An additional advantage is that assumption (5) allows the integration of equations (1-4) to be carried out.

Carrying out the integrations of equations (1-4) and breaking out the linear force and moment terms so that empirical data can be used instead of slender body values gives the following expressions.

$$F_z = -\frac{\pi}{2}\rho_\infty |u| w a_o^2 C_{N_\alpha} - \pi\rho_\infty uq\left[a_o^2(\ell - x_{s,m}) + a_1^2 x_{s,m}\right]$$
$$- \rho_\infty n c_{d_c}\left\{ w\sqrt{v^2+w^2}\cdot I_1 + \left[w\frac{(rv - qw)}{\sqrt{v^2+w^2}} - q\sqrt{v^2+w^2}\right]\cdot I_2 - q\frac{(rv-qw)}{\sqrt{v^2+w^2}}\cdot I_3\right\} \quad (6)$$

$$F_y = -\frac{\pi}{2}\rho_\infty |u| v a_o^2 C_{N_\alpha} - \pi\rho_\infty ur\left[a_o^2(\ell - x_{s,m}) + a_1^2 x_{s,m}\right]$$
$$- \rho_\infty n c_{d_c}\left\{ v\sqrt{v^2+w^2}\cdot I_1 + \left[v\frac{(rv - qw)}{\sqrt{v^2+w^2}} + r\sqrt{v^2+w^2}\right]\cdot I_2 + r\frac{(rv-qw)}{\sqrt{v^2+w^2}}\cdot I_3\right\} \quad (7)$$

$$M = \frac{\pi}{2}\rho_\infty |u| w a_o^2 (x_{s,m} - \bar{x}) C_{N_\alpha} - \pi\rho_\infty uq \left[a_o^2 (\ell - x_{s,m})^2 - a_1^2 x_{s,m}^2 + I_4 \right] + \rho_\infty n c_{d_c} \left\{ w \sqrt{v^2 + w^2} \cdot I_2 + \left[w \frac{(rv - qw)}{\sqrt{v^2 + w^2}} - q \sqrt{v^2 + w^2} \right] \cdot I_3 - q \frac{(rv - qw)}{\sqrt{v^2 + w^2}} \cdot I_5 \right\} \quad (8)$$

$$N = -\frac{\pi}{2}\rho_\infty |u| v a_o^2 (x_{s,m} - \bar{x}) C_{N_\alpha} - \pi\rho_\infty ur \left[a_o^2 (\ell - x_{s,m})^2 - a_1^2 x_{s,m}^2 + I_4 \right] + \rho_\infty n c_{d_c} \left\{ v \sqrt{v^2 + w^2} \cdot I_2 + \left[v \frac{(rv + qw)}{\sqrt{v^2 + w^2}} + r \sqrt{v^2 + w^2} \right] \cdot I_3 + r \frac{(rv - qw)}{\sqrt{v^2 + w^2}} \cdot I_5 \right\} \quad (9)$$

where

$$I_1 = \int_0^\ell a \, dx_s \qquad I_2 = \int_0^\ell a(x_{s,m} - x_s) dx_s$$

$$I_3 = \int_0^\ell a(x_{s,m} - x_s)^2 dx_s \qquad I_4 = \int_0^\ell a^2 (x_{s,m} - x_s) dx_s \quad (10)$$

$$I_5 = \int_0^\ell a(x_{s,m} - x_s)^3 dx_s$$

a_o = radius of the cylindrical portion of the body

$$a_1 = \begin{cases} 0, & \text{if nose is pointed} \\ a_o, & \text{if nose is flat faced} \end{cases}$$

where n, c_{d_c}, C_{N_α} and $\bar{x}$ are to be determined from empirical correlations. To avoid unnecessary computer run time, available methods were reduced to the simplest possible forms which did not sacrifice accuracy substantially[3].

EQUIVALENT ANGLE OF ATTACK FORMULATION FOR FINS

The equivalent angle-of-attack concept is described in detail in References 6 and 7. In brief, the idea is to calculate somehow an equivalent angle of attack, α_{eq}, so that

$$C_{N_i}(\alpha_c, \phi, \delta_1, \delta_2, \delta_3, \delta_4, (\Delta\alpha_{eq})_{v_i}) = C_{N_W}(\alpha_{eq,i}) \tag{11}$$

where

C_{N_i} = normal-force coefficient acting on fin i based on planform area

C_{N_W} = normal-force coefficient acting on wing alone composed of two opposing fins with same exposed planform as fin i joined at the root chords. Reference area is the planform area.

Equation (11) represents an attempt to correlate the variations of the fin normal force due to body angle of attack, body roll angle, and fin deflection through a single parameter, α_{eq}. The quantity C_{N_W} is the wing-alone normal-force coefficient. The wing alone is obtained by removing the body between two opposing fins and joining them together at their root chords. Using experimental values for C_{N_W} allows the incorporation of nonlinear effects.

Consider the side-edge view of a fin shown in Figure 3. The first step is to compute the velocity components V_{p_i} and V_{n_i} seen by the area centroid of the fin. The velocity increments due to body rotation are included. Component V_{p_i} is parallel to the body axis. Component V_{n_i} is perpendicular to the plane the fin would occupy if δ_i were zero.

Due to flow around the body in the crossflow plane, the average normal velocity seen by points on the fin is increased. This phenomenon is known as Beskin upwash[4] and is primarily a function of the shape, angle of attack and Mach number of the body[7].

Using slender body theory, one can show that the ratio of the normal force acting on two opposing fins in the presence of the body with no sideslip and zero fin deflection to the normal force acting on a wing alone composed of the two fins is a function of the ratio of the body diameter to the fin span only. This ratio is called K_W.

For the present work, we shall assume that the effective normal velocity seen by the area centroid of fin i is given by $K_W V_{n_i}$ when the fin is undeflected.

As a first step in the calculation of the effects of fin deflection, we assume that fin i is the only fin on the body (no fin-fin interference). Then the velocity component parallel to the fin root chord is given by

$$V'_{p_i} = V_{p_i} \cos\delta_i - K_W V_{n_i} \sin\delta_i \tag{12}$$

The velocity component perpendicular to the fin is given by

$$V'_{n_i} = K_W V_{n_i} \cos \delta_i + V_{p_i} \sin \delta_i \tag{13}$$

To include vortex effects, the increment in fin normal velocity induced by the trailing vortices from the wing section is added to V'_{n_i} to get

$$V'_{n_i} = K_W V_{n_i} \cos \delta_i + V_{p_i} \left[\sin \delta_i + \sin(\Delta\alpha_{eq})_{v_i} \right] \tag{14}$$

A method for estimating $(\Delta\alpha_{eq})_{v_i}$ is given later in the paper.

To account for fin-fin interference, a factor Λ is applied to the deflection angle of each fin as follows

$$V'_{n_i} = K_W V_{n_i} \cos \delta_i + V_{p_i} \left[\sin(\delta_i \Lambda_i) + \sin(\Delta\alpha_{eq})_{v_i} - \sum_{\substack{j=1 \\ j \neq i}}^{NFINS} \sin(\delta_j \Lambda_j) \right] \tag{15}$$

where NFINS is the number of fins attached to the body at the axial location being considered. Hence, each fin contributes to the equivalent angles of attack of all the other fins in that section. Values for Λ_j obtained from slender body theory are given in Reference 3.

The results of Equations (12) and (15) give α_{eq_i} as follows

$$\alpha_{eq_i} = \tan^{-1} \left(\frac{|V'_{n_i}|}{V'_{p_i}} \right) \tag{16}$$

Then, the force on the fin is given by

$$F_{N_i} = C_{N_W}(\alpha_{eq_i}) \, S_{fin} Q_i V'_{n_i} / |V'_{n_i}| \tag{17}$$

where

$$Q_i = \frac{1}{2} \rho_\infty (V^2_{p_i} + V^2_{n_i}) \tag{18}$$

Methodology for computing the wing-alone normal force coefficient is given in the next section.

FIN NORMAL FORCE

The wing-alone normal-force coefficient for low aspect ratio fins has been correlated in a manner similar to that used by Allen for slender bodies[4]. The equation is

$$C_{N_W} = \frac{1}{2} C_{N_\alpha} \sin 2\alpha \cos \alpha + K \sin^2 \alpha, \qquad 0 \leq \alpha \leq 90° \tag{19}$$

where C_{N_α} is the linear normal-force coefficient slope and K is the drag coefficient of the wing when it is normal to the flow. In general the factor K depends on aspect ratio and Mach number. In Reference 3, correlations for C_{N_α} and K are presented. Also presented are similar correlations for high aspect ratio swept planforms and correlations for longitudinal and lateral positions of the fin center of pressure.

WING-TAIL INTERFERENCE

The method used here for the computation of wing-tail interference is essentially that of Reference 2. However, since that methodology was derived for an unrolled cruciform or monoplane missile, some modification is needed to handle the more general cases encountered for this work. The approach here is to treat the missile as if it were unrolled but with the crossflow velocity equal to $\sqrt{v^2 + w^2}$ and with the wing section developing the actual normal force component which is parallel to and in the same direction as the crossflow velocity vector as seen by the body. The methods of Reference 2 are used to compute an equivalent angle of attack acting parallel to the crossflow velocity vector at the axial location of the tail fin area centroid. That angle of attack is then resolved into components normal to each of the tail fins at their actual orientations. The mathematical details are given in Reference 3.

EXAMPLE CASES

SURFACE-TO-AIR MISSILE

For the surface-to-air missile simulation, it was assumed that the rocket motor had burned out and that the guidance, ordnance and autopilot/battery sections had been separated from the missile as shown in Figure 4. The piece of debris considered was the aft fragment. The computed static margin for the fragment was found to be negative for the transonic and supersonic speed range. Hence, the fragment can be expected to tumble if the control surfaces are not deflected.

Results for the computed trajectory are given in Figure 4. Initially, the missile is in a 10° dive. At $t = t_o$, the forebody is separated. The aft fragment is assumed to be given a slight initial q by the separation event. It immediately pitches up and rapidly tumbles. The velocity of the fragment drops quickly and the aft fragment hits the ground roughly 2,000 feet short of the aiming point. It has been assumed, of course, that the fragment does not disintegrate during the high-q pitch up. It is interesting to note that the trajectory does not appear to be ballistic until $t - t_o = 2$ seconds.

Essentially, this means that downrange travel of the fragment would probably have been underestimated by a two-dimensional computation based on an average drag coefficient.

RYAN BQM-34A TARGET

The geometrical characteristics of the BQM-34A target as given in Reference 8 are shown in Figure 5. The debris fragment to be considered is that portion of the configuration which is aft of the dashed line in the side view (nose and engine gone). Because of the methodology limitations it was necessary to model the body aft of the fragment as a circular cylinder. Three trajectories were run for the BQM aft fragment to illustrate the effect of small changes in the predicted static margin. At the time of separation, the vehicle is assumed to be in level flight at $M_\infty = 0.75$ at an altitude of 500 feet AGL. The computed results are shown in Figure 6. During trajectory #1, the damaged vehicle pitched up to about 1.7° angle of attack and maintained that attitude until impact. During trajectory #2, the vehicle quickly pitched up to 1.5° angle of attack. It continued to slowly increase the pitch attitude until the top of its trajectory at which point the angle of attack was approximately 40°. It then nosed over and fell to the ground. During trajectory #3, the vehicle slowly pitched up to roughly 1° angle of attack. At $t - t_o = 6$ seconds (4,000 feet downrange), it no longer had sufficient speed to maintain level flight and descended until impact.

The "trimmed" flight behavior of the BQM aft fragment as shown in Figure 6 appears to be a result of the tendency of the center of pressure of the fragment to move aft as the angle of attack is increased. Hence, it is possible for there to be an angle of attack, α_o, such that for $\alpha < \alpha_o$ the fragment is unstable. Any slight disturbance would cause the vehicle to pitch to α_o. This phenomenon causes the particular flight behavior encountered to be very sensitive to the center-of-pressure and center-of-gravity locations if the stability of the fragment at small angle of attack is nearly neutral.

SUMMARY

A set of methods has been developed for computing the longitudinal, lateral and control aerodynamic characteristics of a wide range of missile debris fragments. The methods have been incorporated into a computer program which simulates the six-degree-of-freedom trajectories of the fragments. Sample cases presented in this paper and in Reference 3 demonstrate that ballistic, tumbling, coning and "trimmed" flight trajectories can all be predicted for reasonable cost. Typical running times range roughly from 0.5 to 5 times real time on a CYBER 175 computer depending on the complexity of the motion. While the computer program was designed to determine the lethality of a missile once it has broken up, it can also be used for range safety studies.

LIST OF SYMBOLS

a	local radius of body, feet
a_o	radius of cylindrical portion of body alone, feet
a_1	radius of body at $x_s = 0$, feet
C_{N_i}	coefficient of normal force acting on fin i; normal force/$Q_\infty S_{ref}$
C_{N_W}	normal-force coefficient of wing alone formed by putting together two opposing fins at their root chords; normal force/$Q_\infty S_{ref}$
C_{N_α}	derivative of normal-force coefficient with respect to angle of attack, α, at $\alpha = 0$
c_{d_c}	crossflow drag coefficient
F_{N_i}	normal force acting on fin i, lb_f
F_x, F_y, F_z	component in body-fixed coordinate system of force acting on fragment, lb_f
K	drag coefficient of a wing when it is normal to flow
K_W	ratio of normal force acting on two opposing fins in presence of body to normal force of wing alone at same angle of attack as body; no sideslip and no fin deflection
L,M,N	components in body-fixed coordinate system of moment acting on fragment, $ft \cdot lb_f$
ℓ	length of body, feet
p,q,r	components along body-fixed coordinates of rate of rotation of body about its center of mass, radian/sec
$\dot{p},\dot{q},\dot{r}$	rate of change of p, q, r with respect to time, radian/sec^2
Q_i	$\frac{1}{2}\rho_\infty(V_{p_i}^2 + V_{n_i}^2)$
u,v,w	components along body-fixed coordinates of velocity of body center of mass, ft/sec
$\dot{u},\dot{v},\dot{w}$	rate of change of u, v, w with respect to time, ft/sec^2
V_{p_i}	velocity component parallel to body axis at fin i area centroid with no fin deflection, ft/sec
V_{n_i}	velocity component normal to fin i at fin i area centroid with no fin deflection, ft/sec

x_s	rearward distance along body axis from nose tip, ft
$x_{s,m}$	distance from nose tip of fragment to center of mass, ft
$\bar{x}$	axial location of center of pressure measured from nose tip of fragment, ft
α_c	angle of incidence, $\tan^{-1}(V_{CF}/u)$
α_{eq_i}	equivalent angle of attack of fin i
δ_i	deflection angle of fin i
η	parameter accounting for finite length of body, dimensionless
Λ_i	fin-fin interference factor due to deflection of fin i
$(\Delta\alpha_{eq})_{V_i}$	increment in equivalent angle of attack of tail fin i due to presence of vortices shed from wing section
ϕ	missile roll angle, $\tan^{-1}(w/v)$
ρ_∞	atmospheric density, slugs/ft^3

REFERENCES

1. Anon: Baseline Six-Degree-of-Freedom Model. Science Applications, Inc. Report SAI-164-087-252, Sept. 1978.

2. Pitts, W. C., Nielsen, J. N., and Kaattari, G. E.: Lift and Center of Pressure of Wing-Body-Tail Combinations at Subsonic, Transonic, and Supersonic Speeds. NACA TR 1307, 1957.

3. Hemsch, M. J.: Computer Program for Simulating the Six-Degree-of-Freedom Motion of Missile Debris Fragments, Volume I. Methods Development. Nielsen Engineering & Research, Inc., TR-220, July 1980.

4. Nielsen, J. N.: Missile Aerodynamics. McGraw Hill Book Co., 1960.

5. Goodwin, F. K., Dillenius, M. F. E., and Nielsen, J. N.: Prediction of Six-Degree-of-Freedom Store Separation Trajectories at Speeds Up to the Critical Speed. Vol. I - Theoretical Methods and Comparisons with Experiment. AFFDL-TR-72-83, Vol. I, Oct. 1974.

6. Hemsch, M. J., Smith, C. A., Nielsen, J. N., and Perkins, S. C., Jr.: Calculation of Component Forces and Moments of Arbitrarily Banked Cruciform Missiles with Control Deflections. ONR-CR215-226-3, Nov. 1976.

7. Nielsen, J. N., Hemsch, M. J., and Smith, C. A.: A Preliminary Method for Calculating the Aerodynamic Characteristics of Cruciform Missiles to High Angles of Attack Including Effects of Roll Angle and Control Deflections. ONR-CR215-226-4F, Nov. 1977.

8. Jaseniuk, R. P.: Actual Detail Weight Report U.S. Navy Model BQM-34A Aerial Target Drone, Serial Number BQ-19626 Teledyne Ryan Model 124M. Teledyne Ryan Aeronautical Report No. TRA 12444-66, July 1976.

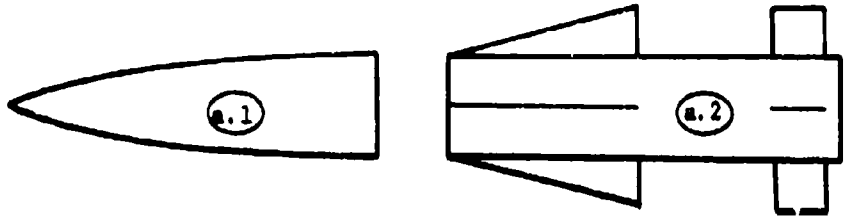

(a) Nose blown off: - a.1 Noses of varying slenderness
a.2 Cylindrical bodies with or without wings and tails

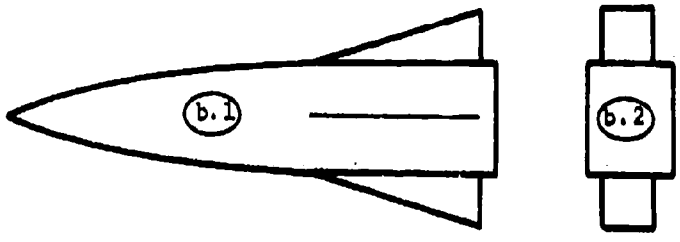

(b) Tail blown off: - b.1 Noses with afterbodies of varying slenderness, with wing section

b.2 Short cylindrical section with tail section

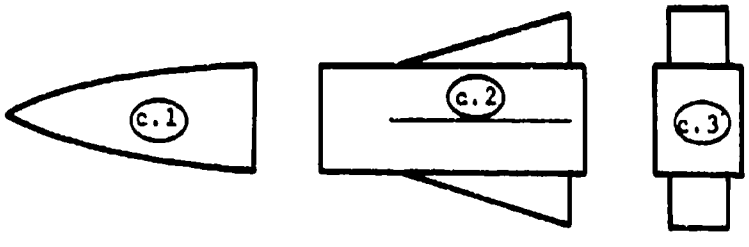

(c) Nose and tail blown off: - c.1 Noses of varying slenderness

c.2 Cylindrical sections of varying length, with wing section

c.3 Cylindrical bodies with wing and tail sections

Figure 1. Possible debris fragment shapes

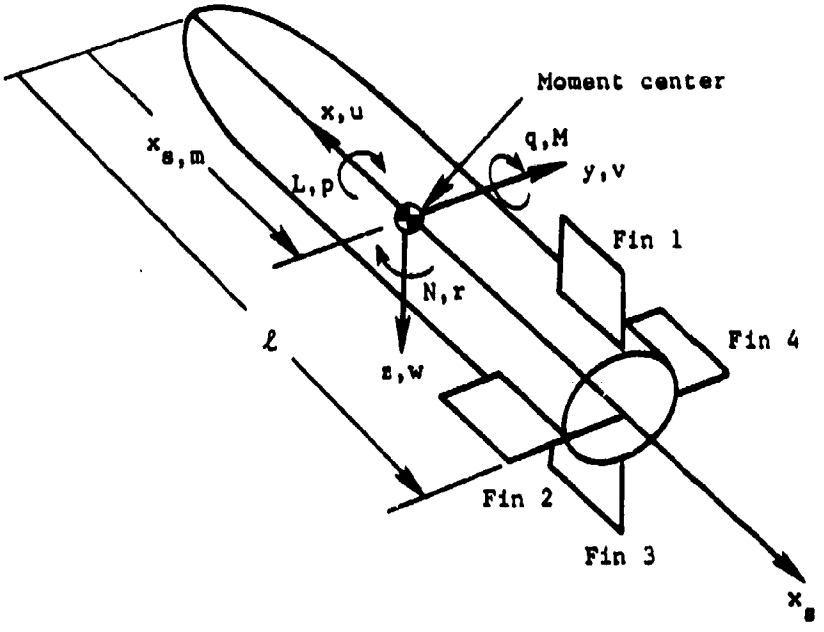

Figure 2. Coordinate system fixed in debris fragment and used in force and moment calculation

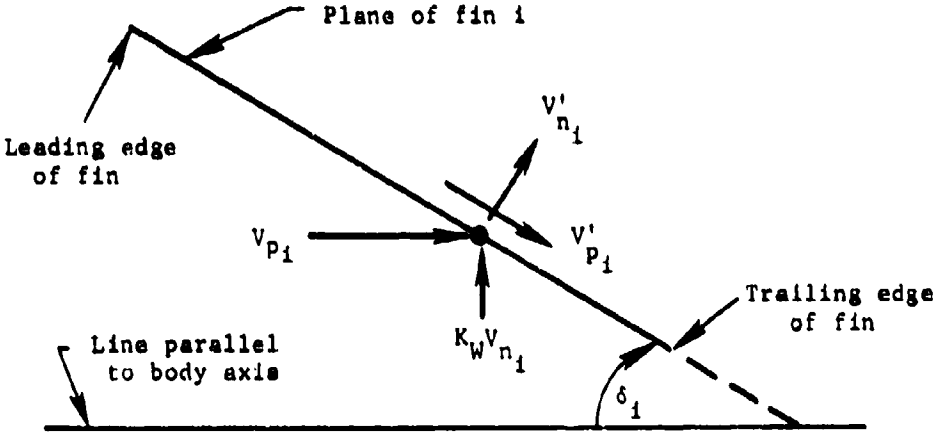

Figure 3. Side-edge view of fin i showing velocity components

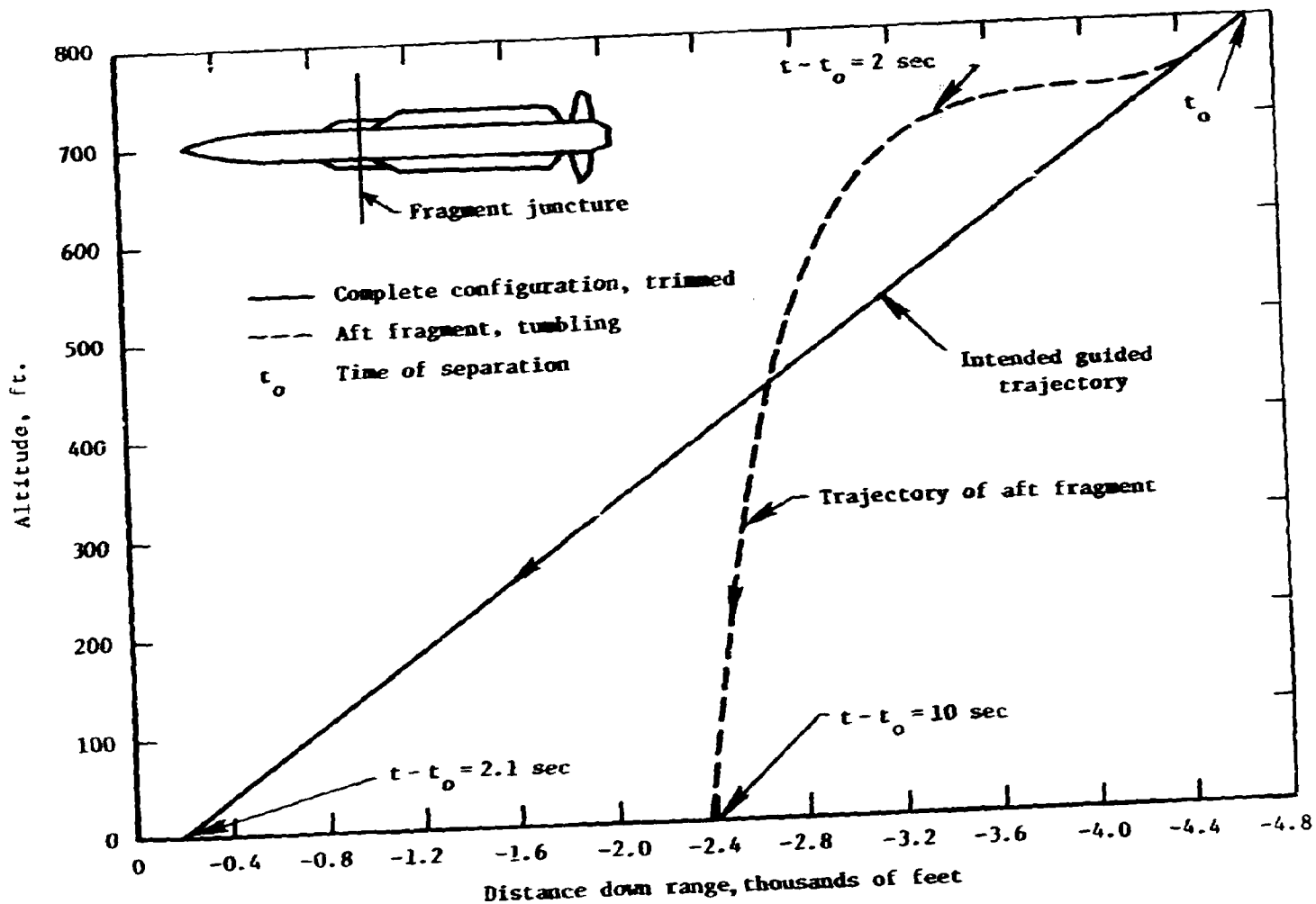

Figure 4. Simulated trajectory of surface-to-air missile

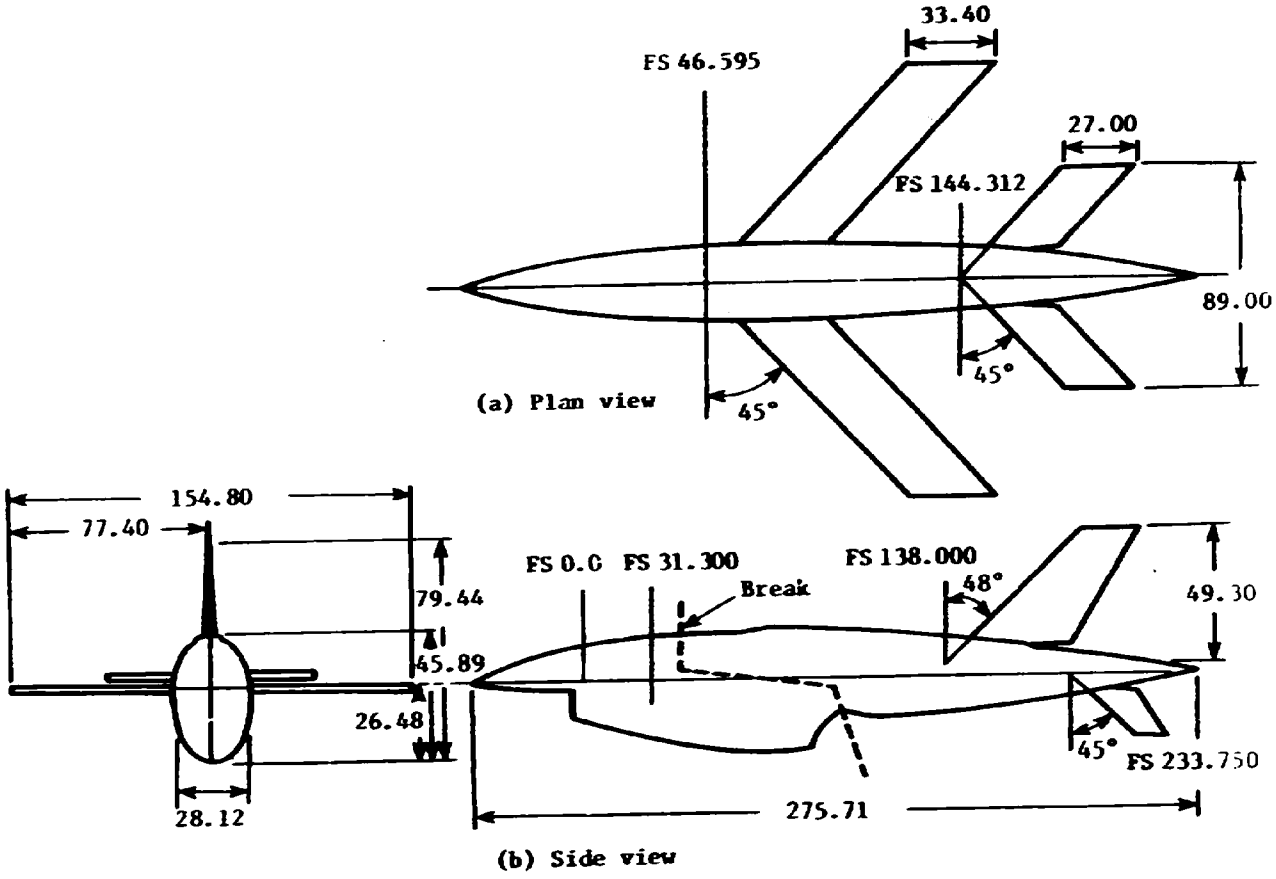

Figure 5. Dimensional data for BQM-34A target
(all dimensions and stations are in inches)

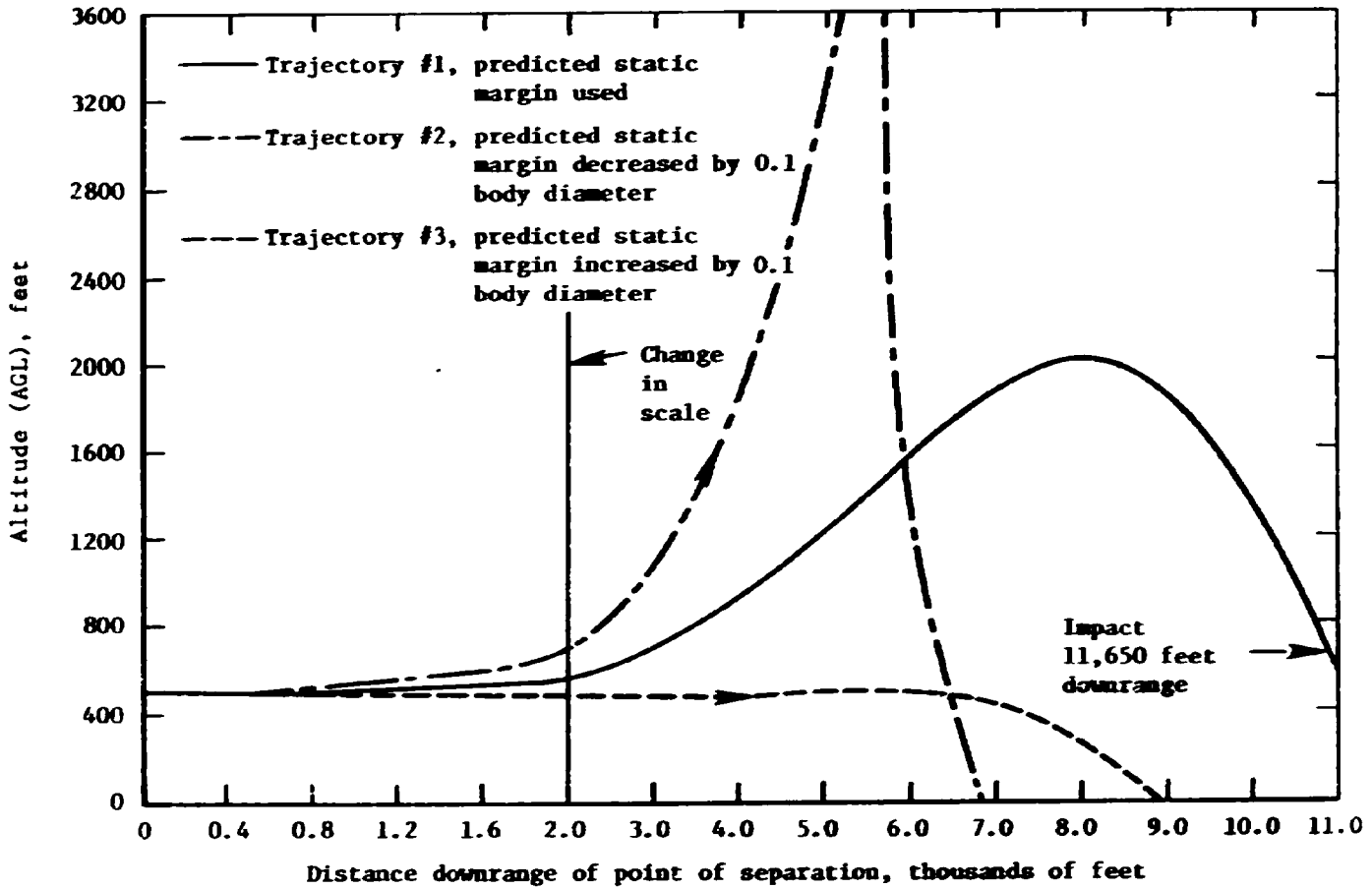

Figure 6. Simulated trajectories of BQM debris fragment